Wideband Channel Sounder With Measurements and Model for the 60 GHz Indoor Radio Channel

Thomas Zwick, *Member, IEEE*, Troy J. Beukema, and Haewoon Nam, *Student Member, IEEE*

***Abstract*—In this paper, a wideband channel sounder and measurement results for the short range indoor 60 GHz channel are presented. The channel sounder is based on a 1 gigasamples/s dual channel arbitrary waveform generator and A/D converter/software demodulator, which synthesize and detect a baseband PN sequence with 500 MHz bandwidth. A heterodyne transmitter and receiver translate the baseband PN sequence to and from the 60 GHz band. Ten channel measurements taken across the 59 GHz to 64 GHz range are concatenated to provide a continuous channel measurement covering 5 GHz of bandwidth, resulting in 0.2 ns time domain channel impulse response resolution. The dynamic range and maximum sensitivity performance of the channel sounder are discussed in detail. Comparisons of results with a vector network analyzer based system are shown to verify the accuracy of the sounder. In an extensive measurement campaign with vertically polarized omnidirectional antennas, several different rooms (offices, labs, conference rooms and others) in four different buildings have been investigated. Over 700 channel measurements are the basis for a comprehensive characterization of the short range 60 GHz indoor radio channel with omnidirectional antennas. Finally, a simple stochastic static multipath channel model is derived from the measurement results.**

***Index Terms*—Channel measurements, indoor radio channel, stochastic channel model, 60 GHz wireless local area network.**

I. Introduction

THE DEMAND for higher data transmission rates is steadily increasing following the introduction and successful deployment of wireless local area networks (WLANs) based on 802.11a/b/g standards in the 2.4 GHz and 5 GHz bands (2.4 GHz, 5.2 GHz and 5.8 GHz). One very interesting option to enable higher data rate systems will be use of the 60 GHz band, which provides a wide available frequency spectrum (e.g., 57 GHz–64 GHz in the U.S. [1]). Especially as an addition to 802.11a/b/g, a 60 GHz WLAN would be a very useful option as discussed in [2]. As with existing 802.11a/b/g WLAN systems, a 60 GHz WLAN application would require omnidirectional coverage. Both the higher carrier frequency and the larger signal bandwidth resulting from high speed data transmission will reduce the coverage range of a 60 GHz system with omnidirectional antennas significantly compared to existing 802.11a/b/g systems. Due to this limited range, a 60 GHz system is more naturally suited for short range, or wireless personal area network (WPAN) applications. Once available, a future system could switch between an 802.11a/b/g and a local 60 GHz access point to provide single user data rates up to 200 Mbps or higher with developing physical layer standards such as 802.15 WPAN high rate alternative [3]. Other examples of high speed short range applications include wireless firewire (e.g., digital camcorder-to-PC connection); wireless docking station (fast Ethernet); and wireless VGA (e.g., a wireless projector connection in conference rooms).

Very important for the optimization of future 60 GHz WPAN system designs (including modulation scheme, coding, radio and antenna design parameters, etc.) is the knowledge of the radio channel in this frequency range. Therefore, in this work, a wideband channel sounder with omnidirectional antennas and better than 1 ns delay resolution was built and used to measure the multipath and loss characteristics of the short range 60 GHz radio channel.

A large variety of different channel measurement setups have been reported to date. One may group them into two major categories [4]:

1) Narrowband Sounding: A vector network analyzer (VNA) is used to measure complex frequency response, which then can be transformed into the channel impulse response (CIR) via Fourier transform [5]–[10]. VNA based channel measurement setups can in principle cover any bandwidth (mostly limited by the antenna bandwidth), but since the frequency points are measured sequentially over a long time span, the method is limited to time invariant channels. In addition, a phase stable RF cable is required between transmitter (Tx) and receiver (Rx), which limits the usability, especially in the millimeter wave (MMW) frequency range.

2) Wideband Sounding: Wideband channel sounding techniques usually involve pulse compression methods, although some earlier systems were based on a short transmitted pulse, which was detected together with all its echoes at the receiver to provide the CIR directly [11]. To improve the dynamic range, newer wideband sounding sytems use pulse compression techniques based on pseudo noise (PN) sequences. Correlation of the received signal with the original transmitted sequence directly yields the CIR. Most systems reported to date use a hardware implementation of a sliding correlator [12]–[14], while some newer systems work with A/D sampling cards and perform the correlation with a microprocessor [4]. In the latter case, an inverse filter obtained from a calibration measurement can replace the correlation [15]. Although wideband sounding techniques are much faster than VNA based systems in terms of measurement time needed for a given time resolution, their major

Manuscript received May 12, 2004; revised September 10, 2004 and December 2, 2004. This work was partially supported by the National Aeronautic and Space Administration. The review of this paper was coordinated by Dr. K. Dandekar.

T. Zwick was with the IBM T. J. Watson Research Center, Yorktown Heights, NY 10598 USA. He is now with Siemens VDO Automotive AG, Weissensberg, Germany.

T. J. Beukema is with the IBM T. J. Watson Research Center, Yorktown Heights, NY 10598 USA.

H. Nam was with IBM. He is now with the Wireless Networking and Communications Group, University of Texas, Austin, TX 78712 USA.

Digital Object Identifier 10.1109/TVT.2005.851354

disadvantage, besides the higher development effort required to construct custom hardware, is the fact that their maximum bandwidth is limited by the bandwidth or speed of the available components (sliding correlator, A/D converter, etc.). Another way of applying pulse compression techniques to the channel sounding problem is given in [16], where an effective continuous wave (CW) radar was built. In [17], [18], a measurement technique based on broadband periodic multifrequency excitation signals and subsequent correlation processing was used to produce the frequency response of the channel.

In order to increase the maximum bandwidth of the wideband sounding method, a principle described in [19] has been applied. With a wideband sounding system, several neighboring frequency bands are measured and then concatenated in the frequency domain to yield a frequency response limited in range only by the front end bandwidth of the radio transceiver. The maximum transmitter and receiver separation distance is not limited by the need for high frequency phase stable cables, which would be required with a vector network analyzer based measurement approach. In this work, only the time-invariant channel was measured. The radio channel can be approximated as stationary if the channel response is slowly varying relative to the time duration of a data transmission interval, which is typical in the indoor environment. In order to obtain a time-invariant channel during the relatively long ($\sim$10 s) measurement interval, care was taken to minimize external motion in the room. A timer was used to trigger delayed capture of the frequency information, enabling the measurements to be taken with no person in the vicinity of the transceivers. Environments with other moving reflectors such as ceiling fans were avoided. Measurement of time-variant channels is also possible with this method by reducing the switching time between the measurements of the different frequency bands, as described in [19]. A review of time variant channels in general can be found in [20].

At 60 GHz, both the free space loss and the relative transmission loss through building materials are much higher than at 2.4 GHz or 5 GHz [21], [22], [14]. For a high data rate short range indoor WPAN as envisioned here, signal blockage by a person becomes a major concern. In [23], a transmission loss of around 20 dB through a person at 60 GHz has been measured. Therefore, in this paper, the effect of blockage of the strongest path in a channel impulse response has been investigated.

An additional advantage of the channel sounding method based on an arbitrary waveform transmitter and software-based demodulator is that, in addition to the channel measurements, modulation schemes can be easily evaluated by concatenating encoded sequences of modulation following the PN sequence used for sounding the channel. Any arbitrary test modulation sequence can be loaded onto the arbitrary-waveform generator (limited only by the depth of sample memory in the D/A and A/D) and then stored to disk from the A/D converter card. Demodulation and decoding can be done offline to find performance of the modulation, enabling direct correlation of modulation performance and channel impulse response. Evaluation of optimum modulation schemes is outside of the scope of this paper, but is a key requirement to complete a 60 GHz wireless system design.

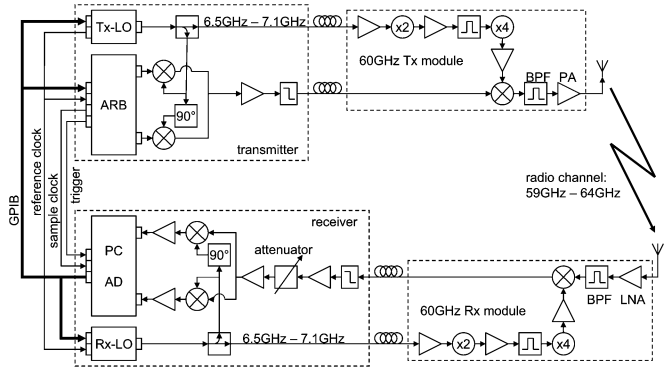

Fig. 1. Channel sounder schematic.

In Section II, the block diagram of the channel sounder is presented with explanations of all key components. Section III describes the method used for system calibration and concatenation of the frequency bands to achieve the full 5 GHz bandwidth. For verification purposes, measurements made with the channel sounder are compared with VNA based measurements in Section IV as shown in [24]. In Section V, statistics of the results of the extensive measurement campaign are presented, and a simple stochastic multipath channel model is proposed. Finally, conclusions are given in Section VI.

II. The Channel Sounder Setup

The channel sounder frequency conversion is based on a heterodyne variable IF concept, which means that both IF and RF mixer frequencies in the conversion chain are varied as the radio is tuned to different RF channels. This enables derivation of the IF and RF local oscillator (LO) signals from the same synthesizer signal so only one synthesizer is required for the transmitter (Tx) as well as for the receiver (Rx). Here, a factor of 8 is used between the two LO frequencies. In Fig. 1, the schematic of the channel sounder is given. An arbitrary waveform generator (ARB) produces a complex baseband signal at 1 gigasamples/s (GS/s) with 10 bits resolution in each channel (I and Q). This signal is IQ modulated onto an IF of approximately 7 GHz, amplified and fed into the 60 GHz Tx module via a 4 m long RF cable. The LO signal for the IQ modulator is generated by a commercial 7 GHz continuous wave (CW) source. The same LO signal is also used for the mixer in the 60 GHz Tx module where it is multiplied by 2 and 4 (for a total multiplication factor of 8) to obtain the correct second LO frequency. A bandpass filter following the initial doubler suppresses the fundamental as well as higher order harmonics, since they would result in unwanted spurious products in the signal after the mixer. A 59 GHz to 64 GHz bandpass filter (BPF) and a power amplifier (PA) with an output 1 dB compression point of approximately 16 dBm connect the mixer output to the antenna in the 60 GHz Tx module. Due to the two flexible cables for IF and LO (both around 7 GHz) the relatively small 60 GHz Tx module can be moved separately from the much larger equipment (mainly ARB and Tx-LO source) comprising the rest of the transmitter. A photo of the 60 GHz Tx module can be seen in Fig. 2.

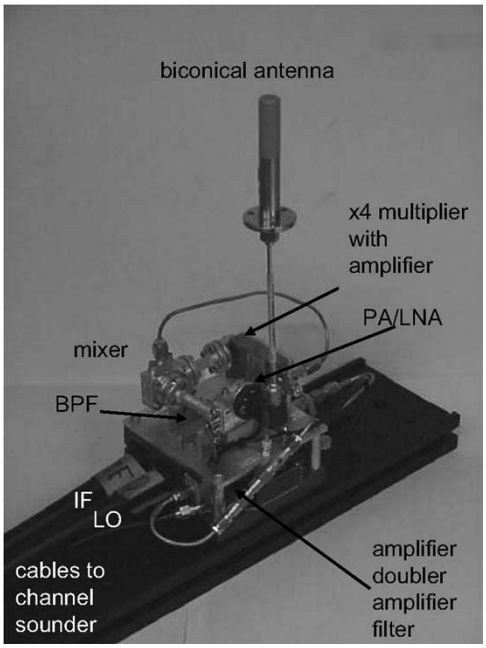

Fig. 2. Photo of 60 GHz Tx module.

At the Rx side, a similar 60 GHz module was used with a low noise amplifier (LNA), replacing the PA in the Tx module. The RF filter, mixer and LO multiplier chain are identical to the Tx module. After some amplification and a variable attenuator (used during calibration), the IF signal is mixed to baseband in an IQ demodulator. The analog baseband IQ signals are amplified and fed into an analog-to-digital conversion card, which can sample complex signals at 1 GS/s with eight bits resolution in each channel (I and Q). The I and Q data is stored in a 4 Mbyte sample buffer memory in the A/D card and transferred to a hard disk under software control. A single LO signal from a 7 GHz synthesizer was used to generate both IF and RF frequency conversions as described above for the transmitter. The noise figure (NF) of the whole receiver is about 6 dB at the LNA input. For this project, vertically polarized biconical horn antennas were designed and built by Flann Microwave Ltd. [25] to achieve a close-to-isotropic radiation. The antenna has an omnidirectional azimuth pattern (± 0.5 dB maximum ripple) and approximately 100° of vertical 3 dB beam width centered in the horizontal plane.

The Tx and Rx equipment is synchronized by connecting the 10 MHz reference clocks of the two synthesizers and the ARB together. The ARB in turn generates a 500 MHz sample clock for the A/D sampling card. This method eliminates time drift between the D/A and A/D, and locks the carrier frequencies of the transmitter and receiver together. A GPIB connection is used to simultaneously switch the LO frequencies at the transmitter and receiver. A trigger signal between the ARB and the A/D sampling card is used to keep the relative timing of data captured in the A/D buffers constant with respect to the phase of the transmitted PN sequence, enabling absolute propagation delay measurement. For all the connections between Tx and Rx (10 MHz reference, sample clock, trigger and GPIB), flexible coaxial BNC cables are used, which can easily be several tens of meters long. For indoor channel measurements, this cable connection between Tx and Rx does not impose any limitations.

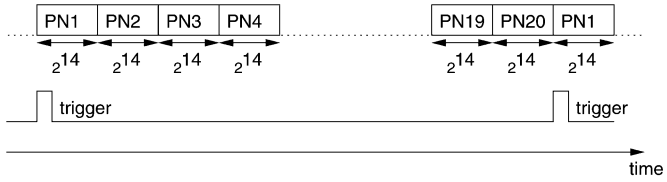

Fig. 3. Time schedule of PN blocks and trigger signal.

III. Calibration and Data Processing

A general description of the radio/propagation channel can be found in [26]–[28]. Here the radio channel is described as a linear, time-invariant system. Antennas are included in the channel and assumed to be isotropic and vertically polarized. In principle, this setup allows time-dependent measurements, but here it was only used for time-invariant measurements to make use of the full 5 GHz bandwidth. Ten sequential channel measurements with a bandwidth of 500 MHz each are performed in the frequency band from 59 GHz to 64 GHz. After calibration, these ten frequency response blocks are concatenated in the frequency domain to one frequency response with 5 GHz bandwidth.

A. Single Frequency Block

First, the method used to obtain the frequency response of one block is described. Two uncorrelated PN sequences (implemented as m-sequences ([29], chapter 8.3) of length 2^{14} are used for I and Q in the ARB. To minimize aliasing effects, a digital 320 tap equiripple low pass filter with a passband of <320 MHz and a stopband of >350 MHz has been applied to the m-sequence. The stopband attenuation of the non-quantized filter is >150 dB. Together with the analog baseband filters, the 3 dB bandwidth of the system in the baseband is about 300 MHz with an equivalent noise bandwidth of approximately 280 MHz.

The channel sounder PN sequence is repeated 20 times to allow noise averaging in the receiver, as shown in Fig. 3. A trigger signal generated by the ARB at the beginning of the first m-sequence is sent to the A/D converter to start the sampling of 20×2^{14} complex samples followed by the data block. Since the m-sequence is much longer than any delay ever expected in the indoor channel, the received m-sequences can be averaged to reduce the noise. Software processing was used to average 18 sequences, followed by a correlation with the ideal m-sequence to generate a complex CIR. From the complex CIR, the frequency response $H(f)$ can be obtained via fast digital Fourier transform (DFT). Since the sequence is much longer than the delay of any multipath component to be expected here, only 125 points out of the CIR are used for the DFT to reduce the noise.

Due to the relatively long IF cables and the very high delay resolution of this channel sounder, multipath/time dispersion effects caused in the channel sounder itself, can be seen in the measurement results. In order to suppress any multipath effects

of the channel sounder itself, a similar technique as in [15] has been applied. In this method, the frequency response of the measurement system itself is first obtained by replacing the two antennas by a coaxial cable and a 36 dB attenuator to directly connect Tx and Rx. For this setup the variable attenuator in the IF path (see Fig. 1) has to be set to 20 dB attenuation to avoid overdriving the IF/baseband circuitry. The measured frequency response $H_{\mathrm{M}}(f)$ of the channel can be corrected using the calibration measurement $H_{\mathrm{cal}}(f)$ performed with the cable between Tx and Rx. This yields the calibrated frequency response of one frequency block

$$H_{\mathrm{C}}(f) = H_{\mathrm{M}}(f) \cdot \frac{H_{\mathrm{cor}}(f)}{H_{\mathrm{cal}}(f)} \tag{1}$$

of the radio channel. $H_{\mathrm{cor}}(f)$ includes the loss and delay of the cable together with the coaxial attenuators used in the calibration measurement and the loss and delay of the antennas with their feed cables, which are removed in the calibration measurement. It was found that $H_{\mathrm{cor}}(f)$ can be fully described by a constant loss a_{cor} and a constant delay τ_{cor} as

$$H_{\mathrm{cor}}(f) = a_{\mathrm{cor}} \cdot e^{-j2\pi f \tau_{\mathrm{cor}}}. \tag{2}$$

This was confirmed by measuring the cable and attenuator with a 65 GHz VNA. The values for a_{cor} and τ_{cor} have been adjusted by placing the antennas at a known distance in a line-of-sight (LOS) environment which clearly with few multipath components and adjusting the loss and delay of the strongest measured path.

Due to the baseband lowpass filtering, only up to around 560 MHz (280 MHz in I and Q channel) of $H_{\mathrm{C}}(f)$ can be used. From the frequency response $H_{\mathrm{C}}(f)$ for one frequency block, the CIR $h_{\mathrm{C}}(\tau)$ can be obtained via inverse digital Fourier transform, which then yields the power delay profile

$$\mathrm{PDP}_{\mathrm{C}}(\tau) = h_{\mathrm{C}}(\tau) \cdot h_{\mathrm{C}}^{*}(\tau) \tag{3}$$

both with a delay resolution of down to 1.8 ns.

From the length of the m-sequence the processing gain can be calculated to be

$$G_{\mathrm{proc}} = 10 \cdot \log(2^{14}) \quad \mathrm{dB} = 42.1\ \mathrm{dB}. \tag{4}$$

Using the equivalent noise bandwidth of $B \approx 560$ MHz, thermal noise power in dBm of

$$P_{\mathrm{therm}} = 10 \cdot \log(kTB) + 30\ \mathrm{dBm} = -86.4\ \mathrm{dBm} \tag{5}$$

at the receiver results (Boltzman constant $k = 1.38066 \cdot 10^{-23}$ J/K, temperature $\mathrm{T} = 293$ K). With the noise figure of the receiver at the antenna $\mathrm{NF} \approx 8$ dB and the averaging factor 18, the system sensitivity yields

$$P_{\mathrm{sens}} = P_{\mathrm{therm}} + \mathrm{NF} - 10 \cdot \log 18 - G_{\mathrm{proc}} = -133.0\ \mathrm{dBm}. \tag{6}$$

Using the transmit power at the antenna $P_{\mathrm{T}} \approx 10$ dBm, the total dynamic range (TDR) of one channel yields

$$\mathrm{TDR}_{\mathrm{C}} = P_{\mathrm{T}} - P_{\mathrm{sens}} = 143.0\ \mathrm{dB}. \tag{7}$$

In addition to the TDR, the instantaneous dynamic range (IDR) is a very important characteristic of a PN sequence based channel sounder. Usually, the processing gain of the PN sequence (4) limits the IDR, but due to the calibration used here (1), the IDR can be better than the 42.1 dB from the processing gain depending on the actual channel and the quantization level at the A/D converter. In order to find the IDR of the system, all collected channel measurements (766 in total) were processed using four times more points than the 125 points used for the noise reduced CIR computation. These extended length CIR responses have a "noise" area at time delays well beyond the decay of channel response to insignificant levels. The IDR can then be estimated as the ratio of total path loss to mean power level in the "noise" section of the CIR. In addition to this mean IDR, a minimum IDR is defined as the ratio of the total path loss to the highest peak in the noise area. The minimum IDR is the range in which a peak can with high probability be considered to belong to the CIR and not to the measurement noise. Both IDRs (500 MHz curves) are given for all measurements in Fig. 4. It can be seen that the mean IDR has a median of about 52 dB and is better than the processing gain G_{proc} in all cases. It can also be seen that the noise peaks are about 10 dB above the average noise floor. Further detailed investigation showed that approximately 15% of the measured channels exhibited IDR substantially worse than the median. In these cases, the system performance was limited by the TDR.

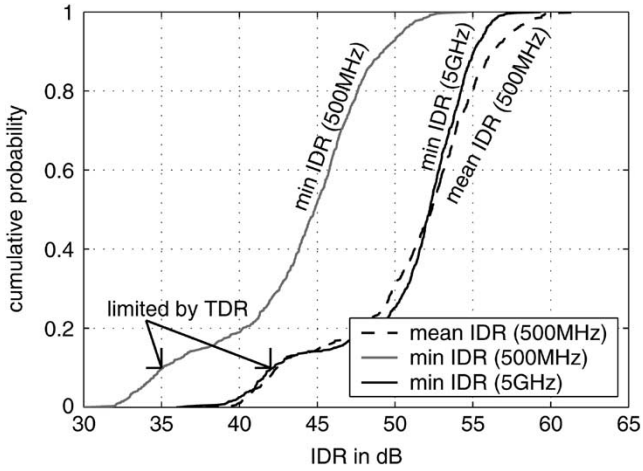

Fig. 4. Instantaneous dynamic range (IDR) of the channel sounder system.

B. Frequency Concatenation

In order to increase the bandwidth of the channel sounder to 5 GHz, ten measurements are performed as explained above, stepping the center frequency in 500 MHz steps over the 59 GHz to 64 GHz range. Using 500 MHz span around the center frequency (-250 MHz to $+250$ MHz) of each measured block, the ten blocks are concatenated to the full 5 GHz wide frequency response $H(f)$. Fig. 5 shows the ten frequency responses measured through the calibration cable before and after calibration. In the uncalibrated curve the baseband frequency response can be seen in each frequency block overlaid by the nonideal frequency response of the MMW transceiver modules. After the calibration, the frequency response is flat to within 1 dB

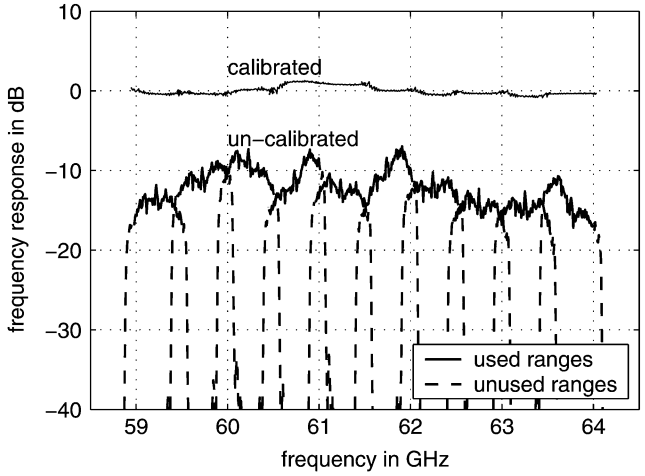

Fig. 5. Amplitude of uncalibrated frequency responses through the calibration cable.

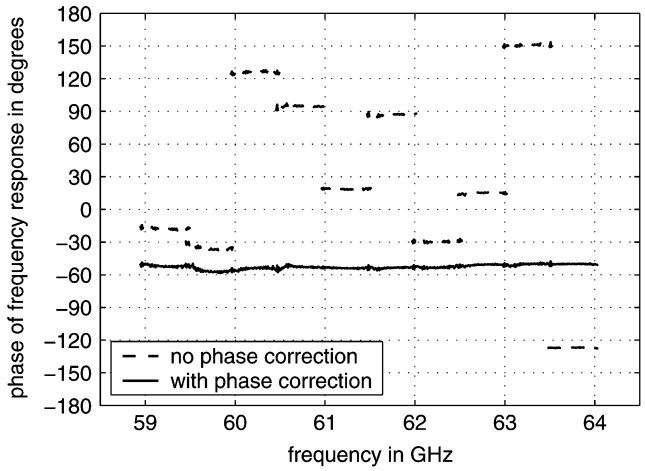

Fig. 6. Phase of calibrated frequency response for measurement of the cable with and without phase correction ($2\pi f \cdot 1.835$ ns has been added to the phase to compensate slope caused by antenna feed lengths which are included in calibration function).

accuracy. As mentioned in Section II the trigger signal assured that the time reference for each of the ten blocks was consistent. However, since different LO sources are used at Tx and Rx and their phased locked loop (PLL) circuits are relocked to arbitrary absolute phases each time the center frequency is changed, all ten frequency responses have arbitrary phase offsets. By using a few frequency points in the overlapping area between the first two measurement blocks the difference between their offset phases is determined and added to the phase of the frequency response data of all blocks after the first one. This procedure is then sequentially performed on all following frequency blocks to allow a proper concatenation. Fig. 6 shows the phase of the final frequency response $H(f)$ after concatenation with and without phase correction.

Since the noise in the ten frequency bands can be expected to be uncorrelated, the frequency concatenation will enhance the TDR of the channel sounder by another 10 dB for a maximum of 153.0 dB. In separate measurements with the transmitter

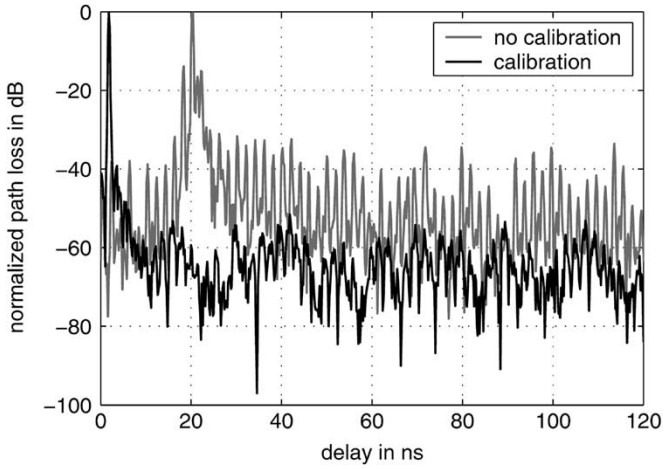

Fig. 7. Uncalibrated and calibrated PDP for ideal channel.

switched off, a TDR of about 148 dB has been observed which confirms the theoretical calculations above. The small discrepancy can be easily explained by the highly varying gain over frequency (see Fig. 5), which results in different TDRs for each different frequency band. This reduces the theoretical gain of 10 dB for the concatenation. As for the IDR, the TDR has to be reduced by about 10 dB to ensure that no peak from the CIR estimate used in the statistical analysis of the data could be a noise peak. Therefore, the maximum measurable path loss of the final system can be given as -138 dB, which easily allows channel measurements within the desired radius (2 m–10 m) without being limited by noise. The frequency concatenation also increases the IDR by about 10 dB as can be seen in Fig. 4. The minimum IDR of the final system has a median of 52 dB and is better than 40 dB in all cases. Fig. 7 shows the normalized power delay profile (PDP) of an ideal channel (obtained by remeasuring with the cable used in the calibration measurement) with and without calibration. In this case the calibration improves the mean IDR from 48.7 dB to 64.4 dB, while also removing the multipath artifacts caused by the measurement system itself. In the uncalibrated result artifacts of up to -15 dB can be seen right beside the main peak.

The frequency concatenation resulted in a total of 625 frequency points, which covered the range from 59 GHz to 64 GHz with a resolution of 8 MHz. This provided a delay resolution of 0.2 ns, enabling separation of paths which are more than 0.4 ns (corresponding to 12 cm) apart. Due to the 8 MHz frequency resolution, the maximum delay or delay unambiguity was 125 ns. This corresponds to 37.5 m in path length, and was sufficient in all performed measurements, since all multipath components decayed to negligible levels over time spans less than 125 ns. If required, the maximum delay can easily be increased in the system by using more points for the DFT.

IV. Comparison With Vector Network Analyzer Based Measurements

For verification of the baseband data processing including the calibration and frequency concatenation, some measurements

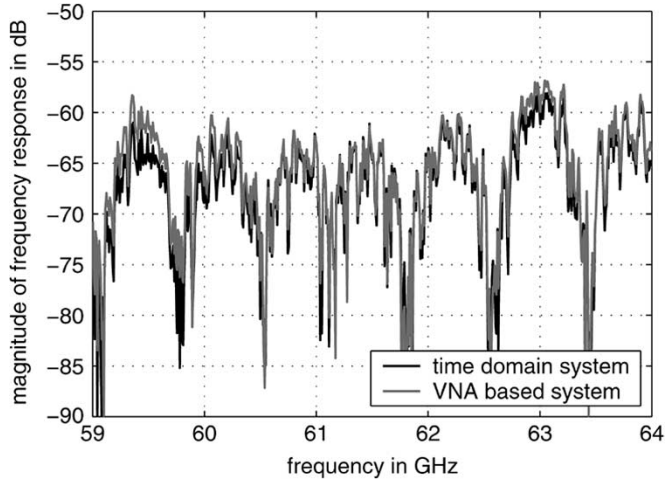

Fig. 8. Magnitude of frequency response measured with the time domain and the VNA based system.

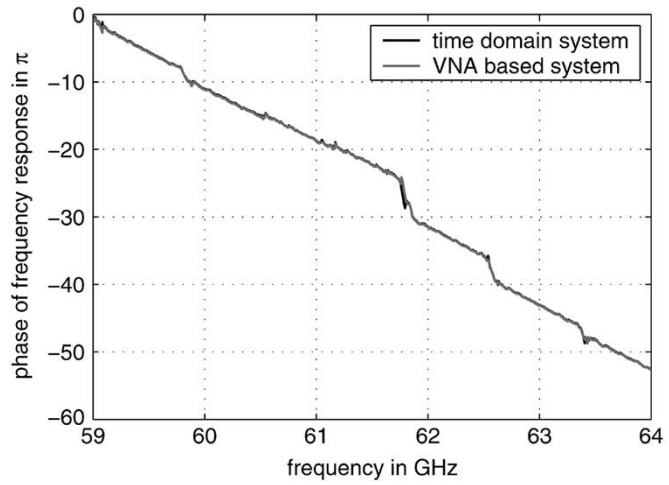

Fig. 9. Phase of frequency response measured with the time domain and the VNA based system.

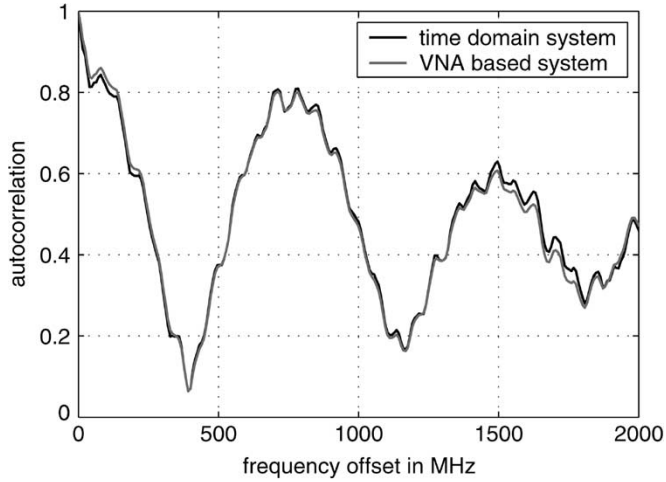

Fig. 10. Frequency autocorrelation measured with the time domain and the VNA based system.

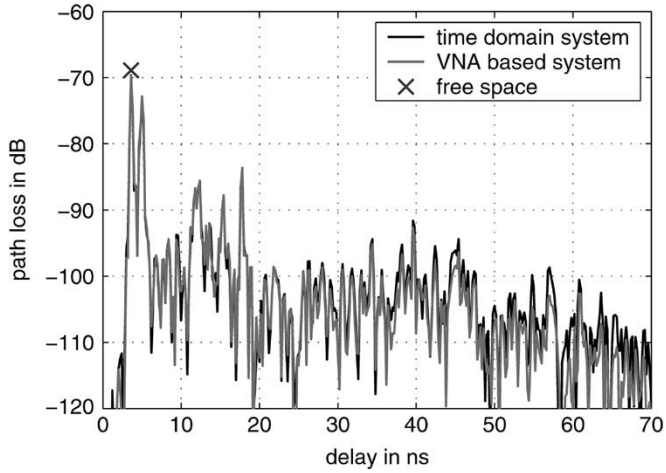

Fig. 11. PDP measured with the time domain and the VNA based system.

were repeated with a VNA based system. To switch to the VNA, GPIB controllable switches were inserted at the IF ports (see Fig. 1) of both Tx and Rx to connect the transceiver IF ports to two ports of a 3 GHz to 8 GHz VNA. This allowed repeating the time domain measurement with the VNA in exactly the same environment through the same IF/RF/antenna hardware. An LO frequency of 7 GHz was used for the 60 GHz transceiver modules to upconvert the 3 GHz to 8 GHz VNA range to 59 GHz to 64 GHz. The measurements have been performed in a laboratory with metallic walls and a lot of measurement equipment, so numerous strong reflections can be expected. Figs. 8 and 9 show the magnitude and phase of the frequency response, respectively. A very good agreement between both measurement systems can be seen (see Fig. 8). The close match of both phase curves in Fig. 9 also demonstrates proper phase concatenation for typical indoor environments with strong multipath behavior (see deep notches in Fig. 8). Other scenarios tested to verify the time domain measurement results with the VNA based system showed similar agreement.

A very important measure to characterize the multipath behavior of a radio channel is the frequency autocorrelation function shown in Fig. 10, which can be derived from the frequency response $H(f)$ by

$$R(\Delta f) = \int_{f_{\min}}^{f_{\max}-\Delta f} H(f)H^*(f+\Delta f)\,df \qquad (8)$$

with $f_{\min}$ and $f_{\max}$ being the minimum and maximum frequencies 59 GHz and 64 GHz of the measured frequency response [30]. It can be seen that in cases like the one if Fig. 10, the coherence bandwidth B_{coh} cannot reasonably be defined at, e.g., the $1/\mathrm{e}$ correlation level, since the autocorrelation crosses the $1/\mathrm{e}$ level more than once. In other cases the correlation does not even fall below the $1/\mathrm{e}$ margin at all. Therefore, the 90% definition is used here for B_{coh}, as in [30].

The most intuitive function to describe the multipath channel is the PDP [26]. In Fig. 11, a very close agreement between both systems, even at longer delays and weaker paths, can be seen. A Kaiser window with $\alpha = 6$ has been applied to the frequency response before Fourier transformation to reduce the sidelobes

in the time domain. The scenario shown here was LOS with a Tx-Rx separation of 1 m. The calculated free space path loss of the LOS path is given in Fig. 11 as reference. The result in Fig. 11 also clearly shows that a resolution of 1 ns is not sufficient for a 60 GHz channel sounder system to be used to characterize the indoor short range radio channel. The two largest peaks in Fig. 11 are just about 1 ns apart, so a system with better than 0.5 ns resolution is required to clearly separate those multipath components.

V. Measurement Results and Channel Model

A total of 766 channels have been measured in several different rooms in four distinct buildings. The first building is the T. J. Watson Research Center. Small offices, conference rooms, the library and a laboratory have been measured. The walls are either made of plasterboard or metal. In the second building, small offices with brick walls have been measured. The third building consists of cubicles in a huge hall. The last building was a private home (wood/plasterboard construction) where two medium size rooms have been measured. The Tx and Rx were always located in the same room but the following three different configurations have been investigated:

- Tx at ceiling and Rx on desk,
- Tx on wall close to ceiling and Rx on desk, and
- both Tx and Rx on desk.

The Tx and Rx separation was varied in the range from 0.5 m to 13 m. The measurements include 373 LOS cases and 393 cases where the LOS was obstructed by, e.g., a monitor or a cubicle separation wall. In the following, statistical results for these measurements are presented and discussed.

A. Delay Spread and Coherence Bandwidth

The most widely used statistical parameter to describe multipath behavior of a radio channel, the root-mean-square (RMS) delay spread τ_{rms}, requires special attention. Its calculation is straightforward since it is the second moment of the PDP [11], ([3], chapter 5). The problem when deriving the RMS delay spread from measured PDPs is to make sure that all relevant paths have been included in the calculation without using noise peaks. Usually a certain threshold below the total received path loss (sum of all paths in the PDP [12]) is used to select the paths to be used for the delay spread calculation. Another method which may be used to select paths for the RMS delay spread computation is to order the paths in power from largest to smallest, then add paths from this ordered list until the summed power of the selected paths reaches a desired percentage of the total power of all paths. In Fig. 12, the cumulative distribution of the RMS delay spread using both definitions is given. The close match of the two curves of the delay spread for a -30 dB threshold and for 95% power usage suggests that both methods yield very similar delay spread numbers on a per-scenario basis. This could be confirmed by the standard deviation of the difference between the delay spreads using a -30 dB threshold and using 95% of the total power, which was only 0.6 ns.

Using 99% of the total power further increases the delay spread of the results shown here compared to the 95% case, but

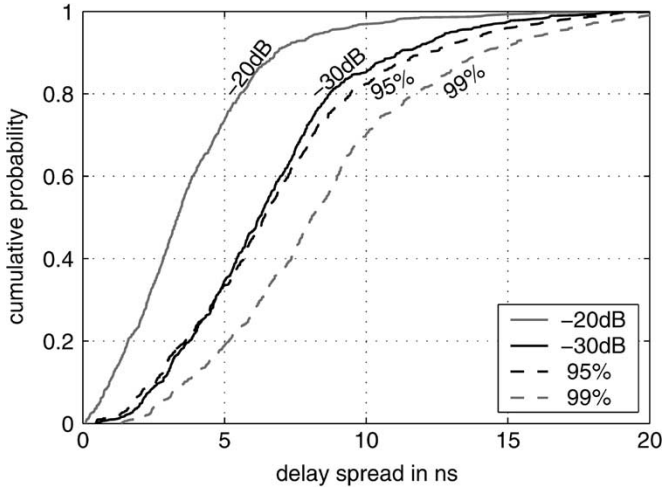

Fig. 12. Cumulative distribution for different delay spread definitions.

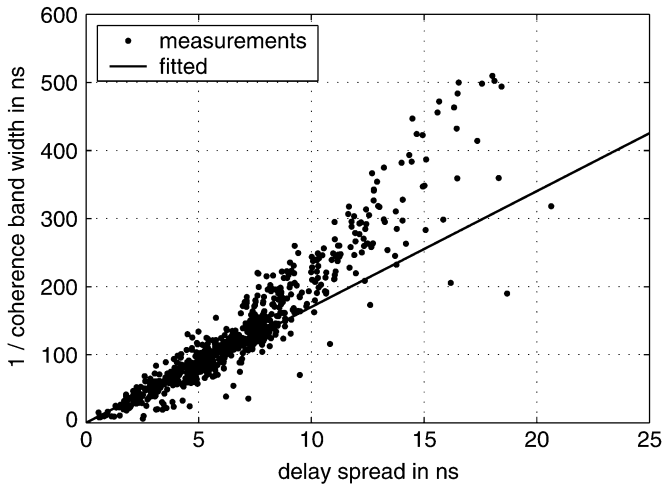

Fig. 13. Inverse of coherence bandwidth versus delay spread using all paths and without the strongest path.

in six out of 766 PDPs peaks below the maximum detected noise level (given by minimum IDR) had to be used to reach 99% of the total power. This leads to the conclusion that in the 60 GHz indoor radio channel, the delay spread from PDPs with infinite IDR would be even higher than the 99% power usage numbers shown here, so no maximum delay spread can be determined. This result is in contrast to measured results in mobile radio channels at lower frequencies, which show that the delay spread value reaches a maximum value far before the threshold used for delay spread calculation reaches the noise floor [32]. Therefore, one has to be very careful when comparing or using delay spread results from different sources without looking at the definition used for calculation, as already realized to some extent in [11] at lower frequencies. In the following, a threshold of -30 dB is used for all RMS delay spread results.

To investigate the relationship between the delay spread and coherence bandwidth, both are plotted against each other in Fig. 13. It can be clearly seen that the product of coherence bandwidth and delay spread is relatively constant, as shown by others in different channels and frequency bands ([33], ch. 3),

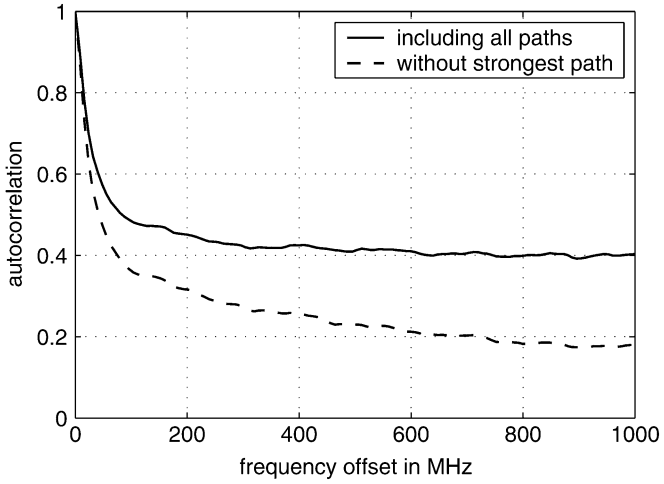

Fig. 14. Mean frequency autocorrelation of all measured scenarios using all paths and without the strongest path.

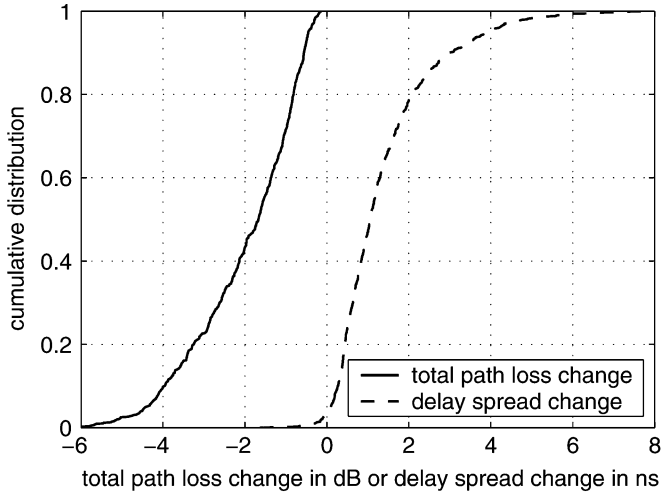

Fig. 15. Cumulative distribution of the change of total path loss and delay spread from using all paths to the same results without the strongest path.

([31], ch. 5). From the data,

$$\tau_{\mathrm{rms}} \cdot B_{\mathrm{coh}} \approx 0.06 \tag{9}$$

was found (only valid for 90% coherence bandwidth and -30 dB threshold RMS delay spread).

B. Blockage of the Strongest Path

As already mentioned in Section I, signal blockage (e.g., by a person) plays a very important role in the 60 GHz WPAN radio channel. Therefore the following statistical results have been computed twice: first with the measurement result as is, and second, after subtracting the strongest path to emulate blockage of the strongest path (which does not have to be the LOS path since LOS only exists in about half of the cases).

Fig. 14 shows the mean frequency autocorrelation (8) averaged over all measured scenarios. It can be seen that eliminating the strongest path reduces the mean autocorrelation floor for large frequency separation from 0.4 to 0.2.

Fig. 15 shows the cumulative distribution of the change of total path loss and delay spread when the strongest path is subtracted from the PDPs. It can be seen that with the omnidirectional antennas used, the total received power drops less than 6 dB in all cases (less than 2 dB in 50% of the cases), while the RMS delay spread increases by up to 6 ns (less than 1 ns in 50% of the cases). This result shows that a wideband, omnidirectional 60 GHz system can take advantage of the multipath behavior of the channel and still operate, in many cases, when the strongest path is blocked. Although the multipath provides resistance against signal blockage, it also contributes significant intersymbol interference distortion at high data transmission rates, which must be addressed using an appropriate modulation/coding design for the channel.

C. Channel Model

Since significantly different delay spreads in the different investigated environments have been observed, the data have been divided into the following three characteristic environments:

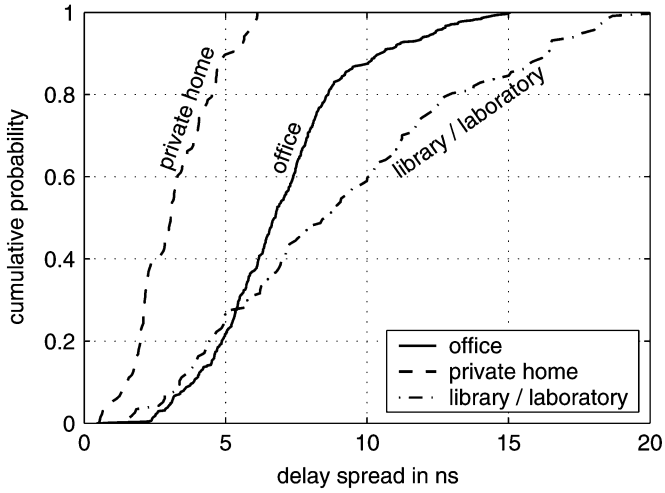

Fig. 16. Cumulative distribution of delay spread for different environments.

- Office (513 PDPs): the office environment groups all office (mostly between 8 m^2 and 12 m^2) measurements including cubicles and conference rooms.
- Private home (136 PDPs): due to the absorptive furniture (couches, carpets, etc.) unique to the private home environment, the measurements in the private home showed much lower delay spreads than all other measurements.
- Library/laboratory (117 PDPs): these two measurement scenarios showed substantially higher delay spreads than the rest of the measurements, which can be explained by the large size of the library and all the highly reflective metallic equipment and walls in the laboratory.

The cumulative delay spread distinguished in the three groups, as explained above, is given in Fig. 16. The hypothesis that room size is a large factor for the delay spread is also supported by results from the literature. In [34], [30], delay spreads of up to 60 ns have been observed in long corridors (25 m–40 m) and large rooms (about 90 m^2). Delay spreads of about 15 ns to 45 ns have been reported in [5] for three different

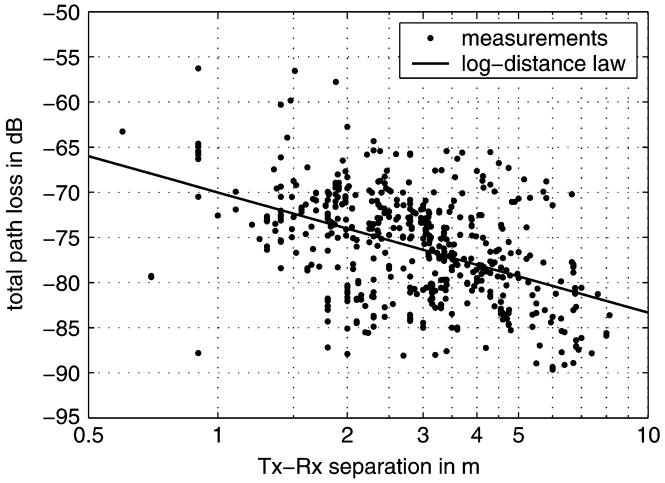

Fig. 17. Total path loss in office environments versus Tx-Rx separation.

rooms of 85 m^2 to 105 m^2 size, where the largest influence on the delay spread was found to be the reflectivity of the walls (the three rooms were approximately the same size). In [14], delay spreads of 10 ns up to 60 ns have been found for two hallways of 54 m and 102 m length while the delay spreads for the four rooms of about 20 m^2 to 60 m^2 size were in the range of 10 ns to 20 ns. In [6], delay spreads of between 3 ns and 10 ns and between 10 ns, and 20 ns in an 18 m long corridor have been measured which correspond well the results presented here.

In the following, a stochastic wideband channel model for the office environment is presented. As already developed for indoor radio channel modeling at lower frequencies [35], [27], the total path loss L can be modeled by a normal distribution in dB (log-normal distribution for linear power path loss) with mean $\mu_{\mathrm{SF}}(d)$ and standard deviation σ_{SF}. In Fig. 17, the total path loss of all measurements in the office scenarios is given over the Tx-Rx separation. This has been verified by dividing the measured data into 6 distance intervals, which also showed the standard deviation σ_{SF} to be consistent over the Tx-Rx separation. The dependence of the mean path loss $\mu_{\mathrm{SF}}(d)$ on the Tx-Rx separation can be described by the so-called log-distance law [35], [27]:

$$\mu_{\mathrm{SF}}(d) = L_{\mathrm{LD,1m}} + 10 \cdot n_{\mathrm{LD}} \cdot \log\left(\frac{1\mathrm{m}}{d}\right). \tag{10}$$

The values for $L_{\mathrm{LD,1m}}, n_{\mathrm{LD}}$, and σ_{SF} have been extracted from the measurements in the office environments (see Table I) using a least-mean-square fit.

In addition to the total path loss model given above, the multipath behavior of the 60 GHz indoor radio channel has to be modeled. Here, a simple stochastic model for generating multipath channels as

$$H(f) = \frac{10^{\frac{L}{20}}}{a_{\mathrm{tot}}} \cdot \sum_{i=0}^{N-1} a_i \cdot e^{-2j\pi f \tau_i} \tag{11}$$

is proposed, where L is the total path loss in dB obtained from the normal distribution (mean from log-distance law) as explained above. The total path loss L is assumed to be statistically independent from the multipath part of the channel. The multipath

TABLE I
MODEL PARAMETERS FOR OFFICE ENVIRONMENTS.

$L_{\mathrm{LD,1m}}$	-70.0dB
n_{LD}	1.33
σ_{SF}	5.1dB
path density λ	0.5/ns
maximum delay τ_{max}	100ns
$\mu_{PV}(\tau)$ for $0 \le \tau < 0.4$ns	0.3
$\mu_{PV}(\tau)$ for $0.4\mathrm{ns} \le \tau$	$0.01 \cdot e^{-0.12\tau/\mathrm{ns}}$

part is then given by the sum in (11), where a_i and τ_i are the complex amplitudes and the delays of the paths $i = 0 \ldots N-1$ (note that N is a stochastic variable as explained in the following). The CIR/PDP can be obtained from the frequency response in (11) via Fourier transform using the same window as in Section IV. Therefore, the bandwidth can be adapted to the system need as discussed in [27]. As proposed in [11], the time between two paths $\Delta\tau = \tau_i - \tau_{i-1}$ is assumed to be exponentially distributed

$$p_{\Delta\tau} = \lambda \cdot e^{-\lambda\Delta\tau}\sigma(\Delta\tau), \tag{12}$$

where $\sigma(\,\cdot\,)$ is the unity step function. Using (12), path delays τ_i can be generated until τ_i exceeds a certain maximum delay, $\tau_{\max}$. The number of paths N will then be Poisson-distributed ([36], chapter 4) with the expectation value

$$\mathrm{E}\{N\} = \lambda \cdot \tau_{\max}. \tag{13}$$

A thorough investigation showed that $|a_i|$ can best be modeled by a Rayleigh distribution or $|a_i|^2$ by a gamma distribution with two degrees of freedom [37] as shown in [27], [38], [32]. The complex path amplitudes a_i can be generated in the model from two normal distributed random variables X and Y, with zero-mean and standard deviation $\sigma_{\mathrm{PV},i}$ as

$$a_i = X + jY. \tag{14}$$

The resulting mean $\mu_{\mathrm{PV},i}$ of $|a_i|^2$ is related to $\sigma_{\mathrm{PV},i}$ by

$$\sigma_{\mathrm{PV},i} = \sqrt{\frac{\mu_{\mathrm{PV},i}}{2}}. \tag{15}$$

The phases of a_i are uniformly distributed. This model assumes that no fast fading has to be attributed to the individual delay bins due to the high number of multipath components, as discussed in [27]. Fast fading of the channel is inherently modeled by the summation of all paths, a_i. To ensure the correct total path loss distribution of the model (11), the multipath part is normalized by

$$a_{\mathrm{tot}} = \sqrt{\sum_{i=0}^{N-1} |a_i|^2}. \tag{16}$$

In order to determine the parameters for the multipath part of the model given above, all measured PDPs have been normalized by their total path loss. The PDPs have also been shifted on the delay axis by setting the delay of the first path

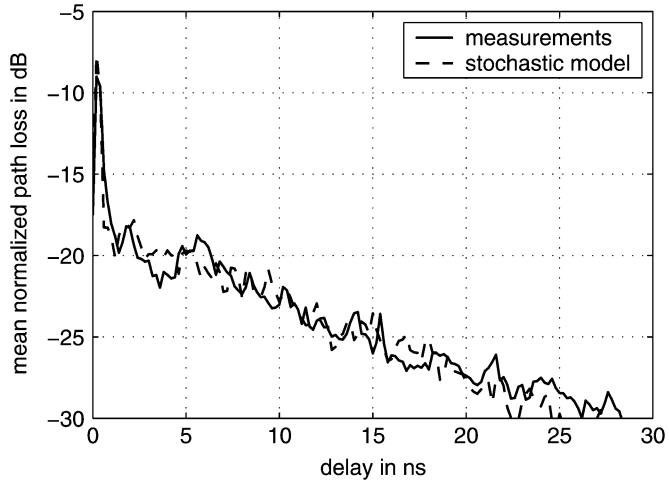

Fig. 18. Average of all normalized PDPs (measurements and model) in the office environment.

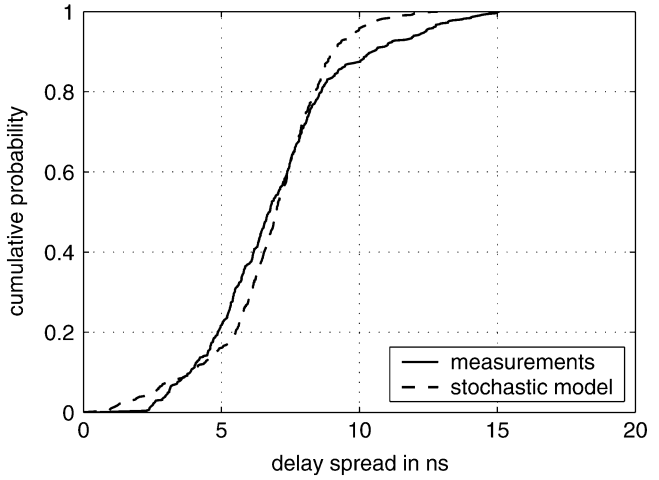

Fig. 19. Cumulative distribution of delay spread (measurements and model) in the office environment.

above -30 dB below the total path loss to zero delay. This time shift does not affect the channel model since the model is designed to match the power delay statistics, not an absolute delay arising from path separation. Grouping the measured data into several Tx-Rx separation ranges showed no significant dependence of the normalized CIR on the Tx-Rx separation. The model parameters have been varied until the mean normalized PDP and the cumulative delay spread distribution from the channels generated from the model best matches the measured results. The frequency responses generated from the model were transferred to PDPs using the same bandwidth and window as the measurements. They have also been normalized in the same way as the measurements to enable a valid comparison. Figs. 18 and 19 show the mean normalized PDP and the cumulative delay spread distribution of the measurements compared to the stochastic model. A good fit of the model to both the normalized PDP and the cumulative distribution of delay spread measurement results was found. The peak over the first delay bins, together with the exponential decay for larger delays shown in the PDP, agrees with the findings in [27]. The determined model parameters are given in Table I.

VI. Conclusion

In this paper, a wideband channel sounder based on PN sequences for the 60 GHz band is presented, which achieves 5 GHz bandwidth using a frequency concatenation concept. The new method is limited to channels which are time invariant across the measurement interval of all concatenated frequency bands. Paths which are more than 0.4 ns apart can be resolved. In addition, transmitter and receiver separation is not limited by high frequency phase stable cables, as would be required with a vector network analyzer based measurement. The system has an instantaneous dynamic range of better than 40 dB, while its maximum measurable path loss is better than 138 dB, assuming no antenna gain. The performance has been verified by comparison with vector network analyzer based measurements in identical environments. To the authors' knowledge, this is the first channel sounder based on pulse compression with a delay resolution of better than 0.5 ns.

In an extensive measurement campaign with vertically polarized omnidirectional antennas, several different rooms (offices, conference rooms, and others) in four different buildings have been investigated. The channel measurement results can be used to optimize the design of future high data rate 60 GHz WPAN systems. The delay spread results show that for operation in the 60 GHz short range omnidirectional channel, modulation systems designed to work in dispersive channels with RMS delay spreads in the range of up to approximately 20 ns will be needed. The median RMS delay spread ranges from 3 to 9 ns, depending on environment. Based on analysis of the measurement data, a simple stochastic multipath channel model for the office environments was proposed. Parameters of the stochastic model were optimized to fit a set of indoor channel measurements. The model showed good match with the power delay and delay spread characteristics of the measured channel results.

Acknowledgment

The authors would like to thank Mr. M. Pauli, a student at the Institut für Höchstfrequenztechnik und Elektronik of the Universität Karlsruhe (TH), Germany, who helped build the channel sounder. Big appreciation goes to Mr. B. Gaucher, Dr. M. Soyuer and Dr. M. Oprysko from the Communications Department at the IBM T. J. Watson Research Center, Yorktown Heights, NY, USA for their friendly support of the project. The authors also would like to thank the IBM team for the helpful discussions, and especially Mr. C. Baks for his great personal engagement during the measurement campaign. Thanks also go to Prof. T. Rappaport from the Wireless Networking and Communications Group at the University of Texas, Austin, TX, USA for the valuable discussions during this work.

References

[1] Federal Communications Commission, *Code of Federal Regulations, Part 15—Radio Frequency Devices Section 15.255: Operation Within the Band 57.0–64.0 GHz*. USA: FCC, Jan. 2001.

[2] P. Smulders, "Exploiting the 60 GHz band for local wireless multimedia access: Prospects and future directions," *IEEE Commun. Mag.*, vol. 40, no. 1, pp. 140–147, Jan. 2002.
[3] IEEEIEEE 802.15 WPAN High Rate Alternative PHY Task Group 3a (TG3a) [Online]. Available: http://ieee802.org/15/pub/TG3a.html, 2004.
[4] P. J. Cullen, P. C. Fannin, and A. Molina, "Wide-band measurement and analysis techniques for the mobile radio channel," *IEEE Trans. Veh. Technol.*, vol. 43, no. 4, pp. 589–603, Nov. 1993.
[5] P. F. M. Smulders and A. G. Wagemans, "Frequency-domain measurement of the millimeter wave indoor radio channel," *IEEE Trans. Instrum. Meas.*, vol. 44, no. 6, pp. 1017–1022, Dec. 1995.
[6] H. Droste and G. Kadel, "Measurement and analysis of wideband indoor propagation characteristics at 17 GHz and 60 GHz," in *IEE Int. Conf. Antennas Propag. (ICAP)*, Eindhoven, The Netherlands, Apr. 1995, pp. 288–291.
[7] T. Manabe, Y. Miura, and T. Ihara, "Effects of antenna directivity and polarization on indoor multipath propagation characteristics at 60 GHz," *IEEE J. Sel. Areas Commun.*, vol. 14, no. 3, pp. 441–448, Apr. 1996.
[8] J. Hübner, S. Zeisberg, K. Koora, J. Borowski, and A. Finger, "Simple channel model for 60 GHz indoor wireless LAN design based on complex wideband measurements," in *IEEE Vehicular Technology Conference*, Phoenix, AZ, May 1997, pp. 1004–1008.
[9] J. Kunisch, E. Zollinger, J. Pamp, and A. Winkelmann, "MEDIAN 60 GHz wideband indoor radio channel measurements and model," in *IEEE Veh. Technol. Conf.*, Amsterdam, Netherlands, Sep. 1999, pp. 2392–2397.
[10] A. Hammoudeh, D. A. Scammell, and M. G. Sánchez, "Measurements and analysis of the indoor wideband millimeter wave wireless radio channel and frequency diversity characterization," *IEEE Trans. Antennas Propag.*, vol. 51, no. 10, pp. 2974–2986, Oct. 2003.
[11] A. A. M. Saleh and R. A. Valenzuela, "A statistical model for indoor multipath propagation," *IEEE J. Sel. Areas Commun.*, vol. 5, no. 2, pp. 128–137, Feb. 1987.
[12] D. Cox, "Delay doppler characteristics of multipath propagation at 910 MHz in a suburban mobile environment," *IEEE Trans. Antennas Propag.*, vol. 20, no. 5, pp. 625–635, Sep. 1972.
[13] C. R. Anderson, T. S. Rappaport, K. Bae, A. Verstak, N. Ramakrishnan, W. H. Tranter, C. A. Shaffer, and L. T. Watson, "In-building wideband multipath characteristics at 2.5 & 60 GHz," in *IEEE Veh. Technol. Conf.*, Vancouver, BC, Canada, Sep. 2002, pp. 97–101.
[14] H. Xu, V. Kukshya, and T. S. Rappaport, "Spatial and temporal characteristics of 60 GHz indoor channels," *IEEE J. Sel. Areas Commun.*, vol. 20, no. 3, pp. 620–630, Apr. 2002.
[15] P. Truffer and P. E. Leuthold, "Wide-band channel sounding at 24 GHz based on a novel fiber-optic synchronization concept," *IEEE Trans. Microw. Theory Tech.*, vol. 49, no. 4, pp. 692–699, Apr. 2001.
[16] G. Løvnes, S. E. Paulsen, and R. H. Rækken, "A millimetre wave channel sounder based on the chirp/correlation technique," in *IEE Colloq. on High Bit Rate UHF/SHF Channel Sounders—Technology and Measurement*, London, UK, Dec. 1993, pp. 1–7.
[17] R. Thomä, D. Hampicke, A. Richter, G. Sommerkorn, A. Schneider, U. Trautwein, and W. Wirnitzer, "Identification of time-variant directional mobile radio channels," *IEEE Trans. Instrum. Meas.*, vol. 49, no. 2, pp. 357–364, Apr. 2000.
[18] T. Zwick, D. Hampicke, A. Richter, G. Sommerkorn, R. Thomä, and W. Wiesbeck, "A novel antenna concept for double-directional channel measurements," *IEEE Trans. Veh. Technol.*, vol. 53, no. 2, pp. 527–537, Mar. 2004.
[19] R. Kattenbach and D. Weitzel, "Wideband channel sounder for time-variant indoor radio channels," in *Millenium Conf. Antennas Propagation*, Davos, Switzerland, Apr. 2000, CD-ROM.
[20] R. J. C. Bultitude, "Estimating frequency correlation functions from propagation measurements on fading radio channels: A critical review," *IEEE J. Sel. Areas Commun.*, vol. 20, no. 6, pp. 1133–1143, Aug. 2002.
[21] B. Langen, G. Lober, and W. Herzig, "Reflection and transmission behaviour of building materials at 60 GHz," in *IEEE Int. Symp. on Personal, Indoor, Mobile Radio Communikations*, The Hague, The Netherlands, Sep. 1994, pp. 505–509.
[22] K. Sato, T. Manabe, J. Polivka, T. Ihara, Y. Kasashima, and K. Yamaki, "Measurements of reflection and transmission characteristics of interior structures of office building in the 60 GHz band," *IEEE Trans. Antennas Propag.*, vol. 45, no. 12, pp. 1783–1792, Dec. 1997.
[23] K. Sato and T. Manabe, "Estimation of propagation-path visibility for indoor wireless lan systems under shadowing condition by human bodies," in *IEEE Veh. Technol. Conf.*, Ottawa, ON, Canada, May 1998, pp. 2109–2113.
[24] D. Tholl, M. Fattouche, R. J. C. Bultitude, P. Melançon, and H. Zaghloul, "A comparison of two radio propagation channel impulse response determination techniques," *IEEE Trans. Antennas Propag.*, vol. 41, no. 4, pp. 515–517, Apr. 1993.
[25] Flann Microwave Ltd.. (2004). Available: http://www.flann.com [Online].
[26] P. Bello, "Characterization of randomly time-variant linear channels," *IEEE Trans. Commun.*, vol. 11, no. 4, pp. 360–393, Dec. 1963.
[27] T. Zwick, C. Fischer, and W. Wiesbeck, "A stochastic multipath channel model including path directions for indoor environments," *IEEE J. Sel. Areas Commun.*, vol. 20, no. 6, pp. 1178–1192, Aug. 2002.
[28] M. Steinbauer, A. F. Molisch, and E. Bonek, "The double-directional mobile radio channel," *IEEE Antennas Propag. Mag.*, vol. 53, no. 4, pp. 51–63, Aug. 2001.
[29] R. E. Ziemer and R. L. Peterson, *Digital Communications and Spread Spectrum Systems*. New York, NY: Macmillan Publishing Company, 1985.
[30] M. O. Al-Nuaimi and A. G. Siamarou, "Coherence bandwidth characterization and estimation for indoor Rician multipath wireless channels using measurements at 62.4 GHz," in *IEE Proc. Microw. Antennas Propag.*, vol. 149, no. 3, Jun. 2002, pp. 181–187.
[31] T. S. Rappaport, *Wireless Communications: Principles and Practice*. Upper Saddle River, NJ: Prentice Hall, 2001.
[32] *Digital Land Mobile Radio Communications*. Brussels, Belgium: COST Telecom Secretariat, European Commision, 1989. COST 207.
[33] N. Geng and W. Wiesbeck, *Planungsmethoden für die Mobilkommunikation—Funknetzplanung unter realen physikalischen Ausbreitungsbedingungen*. Berlin: Springer, 1998.
[34] A. G. Siamarou and M. O. Al-Nuaimi, "Multipth delay spread and signal level measurements for indoor wireless radio channels at 62.4 GHz," in *IEEE Veh. Technol. Conf.*, Rhodes, Greece, May 2001, pp. 454–458.
[35] J. M. Keenan and A. J. Motley, "Radio coverage in buildings," *British Telecom. Technol. J.*, vol. 8, pp. 19–24, Jan. 1990.
[36] A. Papoulis, *Probability, Random Variables and Stochastic Processes*. New York, NY: McGraw-Hill, 1991.
[37] J. G. Proakis, *Digital Communications*. New York, NY: McGraw-Hill, 1989.
[38] R. Kattenbach, "Charakterisierung Zeitvarianter Indoor-Funkkanäle anhand Ihrer System- und Korrelationsfunktionen," Ph.D. Dissertation, Universität Gesamthochschule Kassel, Germany, 1997.

Thomas Zwick (M'00) received the Dipl.-Ing. and the Dr.-Ing. degrees from the Universität Karlsruhe (TH), Germany in 1994 and 1999, respectively.

From 1994 to 2001 he was research assistant at the Institut für Höchstfrequenztechnik und Elektronik (IHE) at the Universität Karlsruhe (TH), Germany. Between February 2001 and September 2004 he was with the IBM T. J. Watson Research Center in Yorktown Heights, NY, USA. Since October 2004 T. Zwick is with Siemens VDO Automotive AG, Weissensberg, Germany.

His research topics include wave propagation, stochastic channel modeling, channel measurement techniques, material measurements, microwave techniques, wireless communication system design and millimeter wave antenna design.

He participated as an expert in the European COST231 *Evolution of Land Mobile Radio (Including Personal) Communications* and COST259 *Wireless Flexible Personalized Communications*. For the Carl Cranz Series for Scientific Education he served as a lecturer for *Wave Propagation*. He received the best paper award on the Intern. Symp. on Spread Spectrum Techn. and Appl. ISSSTA 1998.

Troy J. Beukema received the B.S.E.E. and M.S.E.E. degrees from Michigan Technological University, in 1984 and 1988, respectively.

From 1984 to 1988 he was a R&D engineer with Hewlett-Packard in the area of communications test equipment. He joined Motorola in 1989 and contributed to development of digital cellular wireless systems with a focus on digital signal processing algorithm design and implementation. In 1996, he joined IBM, where he is presently a research staff member concentrating in the areas of radio architecture and modulation for 60 GHz wireless systems and receiver system design for adaptive equalization of 6–12 Gb/s wireline serial I/O links. His research interests include communication link system design and simulation, with an emphasis on modulation and equalization for wireless and high speed wireline channels.

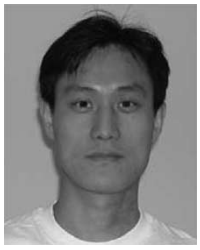

Haewoon Nam (S'99) received the B.S. degree in electrical communication engineering from Hanyang University, Seoul, Korea in 1997 and the M.S. degree in electrical engineering from Seoul National University, Seoul, Korea, in 1999. He is currently working toward the Ph.D. degree in electrical and computer engineering at the University of Texas, Austin.

From 1999 to 2002, he was a member of technical staff in the Telecommunication Research Center, Samsung Electronics, Suwon, Korea, where he was engaged in the design and development of CDMA, GSM/GPRS baseband processors for mobile handsets. In the summer of 2003, he was with the IBM T.J. Watson Research Center, Yorktown Heights, NY, where he performed extensive radio channel measurements at 60 GHz. His research focuses are all areas of wireless communications including performance analysis of diversity systems and radio propagation channel modelling.

He is a recipient of a Korean government fellowship for his doctoral studies in the field of electrical engineering.